

# A versatile dielectron trigger for nucleon-nucleon and nucleus-nucleus collisions.

R. Schicker<sup>1</sup>, M. Axiotis, H. Tsertos

*University of Cyprus, Nicosia, Cyprus*

---

## Abstract

A novel approach for a versatile first level dielectron trigger is presented. This trigger operates in the low multiplicity environment of nucleon-nucleon reactions as well as in the high multiplicity situation of nucleus-nucleus collisions. For optimal trigger performance, time of flight conditions for the two fastest particles of the event are combined with event multiplicity requirements. The dielectron trigger efficiency is given. The event reduction factor of such a trigger approach is studied for a low, a medium and a high multiplicity environment. The impact parameter dependence of the event reduction is given. The timing properties of the trigger signal are described. The losses due to deadtime are specified. Finally, the first level trigger rate is reported.

---

<sup>1</sup> Corresponding author, e-mail "schicker@alpha2.ns.ucy.ac.cy"  
Dept. Nat. Science, Univ. Cyprus, PO 537, 1678 Nicosia, Cyprus

## 1 Introduction

Dielectrons are of particular interest in the study of nucleon-nucleon and nucleus-nucleus collisions since they do not undergo strong final state interactions. The measurement of dielectron observables thus reveals information which otherwise cannot be obtained by measuring hadronic degrees of freedom[1,2]. Dielectrons are, however, produced with cross sections which are typically 4-5 orders of magnitude smaller than pion production cross sections. A large geometrical spectrometer acceptance and maximum beam intensity are therefore necessary in order to measure dielectron observables efficiently. Redundant lepton identification is mandatory for measuring the small dielectron signal in the large hadronic background. In particular, the identification of electrons at the trigger level requires a sophisticated trigger scheme. The rate reduction required from the trigger system can only be achieved by a multi-level trigger architecture.

## 2 Trigger concepts

### *2.1 Conventional triggers*

A first level trigger is usually designed as a reaction trigger. In low multiplicity environments such as in hadron induced reactions, a multiplicity condition of two can be used for the first level trigger[3,4]. This minimum condition of two represents the two partners of the pair. In high multiplicity environments such as in heavy-ion induced collisions, different multiplicity conditions can be used to define a trigger. This trigger tags the events according to their charged particle multiplicity, and hence allows to accept or reject event classes of a given impact parameter range. A minimum multiplicity condition enables the measurement of the minimum bias multiplicity distribution. This minimum bias distribution is used to correct for the multiplicity trigger bias in order to study the impact parameter dependence of the dielectron yield[5].

More restrictive trigger decisions can be made by using detector systems which combine a high electron detection efficiency with a high hadron rejection power as is the case in Cherenkov detectors, for example. If the detector signal is prompt as in threshold gas Cherenkov counters, then this information can be used in the first level trigger[3]. If a higher hadron rejection power is needed, then Ring Imaging Cherenkov counters (RICH) can be used. However, the time scale of the ring pattern search does not allow the inclusion of RICH information in the first level trigger decision. Thus, RICH detector information is generally used in higher level triggers[6,7].

Electron identification on the trigger level can alternatively be achieved by using time of flight (TOF) or calorimetric information. The complexity of electron identification in a large hadronic background, however, restricts TOF or calorimeter information in general to higher level trigger decisions[8,9].

## *2.2 The electron time of flight trigger*

The new trigger concept presented in this paper allows a much improved first level trigger performance by integrating preliminary electron identification into the first level trigger. This preliminary electron identification is based on isochronous TOF information, and is therefore complementary to the information from prompt Cherenkov counters. Thus, this novel approach combines a conventional first level reaction trigger with aspects of traditional higher level electron triggers. Moreover, this new first level trigger approach operates in low as well as in medium to high multiplicity environments.

This novel electron TOF trigger is of practical interest for dielectron spectrometers of any magnetic field configuration. A highly segmented TOF system is, however, a prerequisite for spectrometers of large geometrical acceptance. This TOF segmentation is required for optimizing electron isochronicity within the solid angle covered by the spectrometer. Electron isochronicity is achieved by adding delays to the signal of each TOF segment. These delays compensate for the variations in trajectory length within the acceptance of the spectrometer. The delayed signals are, however, prompt on the time scale of the first level trigger.

## *2.3 Electron time of flight trigger simulations*

In order to study the performance of such a trigger approach, simulations were carried out by taking the dielectron spectrometer HADES at GSI as a specific example. The HADES experiment combines a large geometrical acceptance with a highly segmented TOF array[10]. The performance of such a trigger architecture is studied for a low, a medium and a high multiplicity environment. In particular, the performance of this new trigger approach is compared to the performance of the corresponding first level trigger which does not identify electron candidates.

HADES is designed to operate at heavy-ion and proton beam intensities of  $10^8 \text{ s}^{-1}$ . A 1% interaction target results in  $10^6 \text{ s}^{-1}$  minimum bias events. The maximum available pion beam intensity, on the other hand, reaches values of about  $2 \times 10^7$  per spill at a momentum of 1 GeV/c. The proton beam is therefore more demanding on the first level trigger as compared to the pion

beam. Thus, simulations have been carried out only for heavy-ion and proton induced reactions. The average charged particle multiplicity is higher in proton-nucleus than in proton-proton collisions, and hence heavy-ion targets are more demanding on the trigger system as compared to proton targets. Simulation results are therefore shown below for the systems p+Ni at 2 AGeV, Ne+Ne at 2 AGeV and Au+Au at 1 AGeV as examples of a low, a medium and a high multiplicity environment, respectively. Studies of the high multiplicity system Ni+Ni confirm the conclusions drawn from the above three systems[11].

This paper is organized as follows: Section 3 gives a summary of first level trigger requirements. In Section 4, the simulation of the first level trigger data is described. Section 5 introduces the analysis of the simulation data. Section 6 reports on the first level trigger in the low multiplicity reaction p+Ni. Section 7 gives details of the first level trigger performance in the medium multiplicity system Ne+Ne. In Section 8, the performance characteristics of the first level trigger in the high multiplicity system Au+Au is presented.

### 3 First level trigger requirements

#### 3.1 Hadron induced reactions

A reaction trigger for hadron induced collisions can be defined by requiring a multiplicity condition of two or larger. This minimal multiplicity value of two corresponds to the two charged leptons of the pair. To illustrate this point, we mention here the  $p(\pi^-, e^+e^-)n$  reaction which is tagged by a multiplicity condition of two. This reaction attracts considerable interest for the investigation of the time-like nucleon form factor below the threshold accessible in nucleon-antinucleon annihilation. If the reaction channel to be measured contains additional charged tracks, then the imposed multiplicity condition can be correspondingly increased. Thus, a versatile first level trigger for hadron induced reactions is characterized by a multiplicity condition of two or larger.

In the HADES spectrometer, the multiplicity condition for the first level trigger can be derived from the highly segmented TOF system. In combination with a timing signal of an additional start detector, the TOF trigger signal is used to establish gates for ADCs and to define START/STOP signals for TDCs. Hence the delay of the TOF trigger signal with respect to the time of reaction as well as the time jitter are of particular interest. The time jitter of the first level trigger signal arises from different sources. First, velocity variations of the particles defining the trigger transition induce particle time of flight variations. Second, trajectory length variations over the acceptance of

the spectrometer add to the time of flight variations. Third, different signal propagation times in the TOF elements depending on location of the hit point add varying delays to the TOF signals.

A multiplicity condition of two is triggered by the two fastest particles of the event. For events containing dielectrons, the two fastest particles are the two electrons ( $\gamma \geq 20$ ) of the pair. The contribution to the time jitter due to particle velocity variations mentioned above therefore vanishes. Thus, for a multiplicity condition of two, the trigger time jitter of dielectron events is considerably reduced as compared to events without dielectrons. This time correlation allows to define a timing window  $\Delta T_0$  for the trigger signal derived from the two fastest particles of the reaction. Events containing a dielectron will meet this condition, but most of the events without dielectrons will not. The trigger time jitter of dielectron events therefore contains only the contributions of trajectory lengths variations and of different signal propagation delays as described above. In a highly segmented TOF system, however, trajectory length variations within one TOF paddle are very much reduced as compared to the variations within the full spectrometer acceptance. The differences in the mean TOF value from paddle to paddle can, however, be corrected by cable delays. Thus, the mean electron TOF values (including cable delays) of all TOF paddles are isochronous. The remaining trigger time jitter is dominated by the varying signal propagation delays depending on the hit location within the TOF paddle. In a paddle geometry with readout on both sides, this jitter contribution can, however, be minimized by a mean timer circuit.

The cable delays of the individual TOF paddles and the mean timer improve the trigger time correlation of dielectron events considerably. The timing window  $\Delta T_0$  described above can therefore be narrowed, and less events without dielectrons will initiate a trigger. The deadtime of the first level trigger is therefore reduced considerably. Such a timing window  $\Delta T_0$  necessitates, however, an independent measurement of the reaction time by another detector system. This additional detector system is the start detector mentioned above.

### *3.2 Heavy-ion induced reactions*

A first level trigger in heavy-ion induced reactions tags the events according to their charged particle multiplicity. The correlation between impact parameter and charged particle multiplicity enables the selection of impact parameter ranges by defining corresponding multiplicity conditions. This multiplicity can be derived from a highly segmented detector system. In the case of the HADES spectrometer, the highly segmented TOF array is used.

The six fold azimuthal segmentation of the HADES setup allows for two pos-

sible definitions of a multiplicity trigger. A lower limit on multiplicity in each of the six sectors defines a sector multiplicity condition. Alternatively, a lower limit on the multiplicity summed over the six sectors defines a total multiplicity condition. For central heavy-ion reactions, these two different multiplicity conditions are expected to be equivalent due to the azimuthal symmetry of the reaction zone. For semi-central or peripheral reactions, however, these two conditions are not equivalent due to azimuthal anisotropies of the reaction.

The minimal sector multiplicity for defining a trigger is equal to one. Sector multiplicity conditions can therefore be used for systems which have a small probability to have no tracks in one or more of the azimuthal segments. We define a high multiplicity environment by the property that a sector multiplicity condition of one results in an efficiency loss of less than 10% for central events. These central events exhibit azimuthal symmetries to a high degree. The multiplicity distribution of one azimuthal segment can therefore be approximated by a Binomial distribution  $B(n_S, n_T, p)$ . Here,  $n_S$  and  $n_T$  are the multiplicity in one segment and the total multiplicity, respectively. The parameter  $p$  represents the probability that a single track is located in the segment under consideration. In absence of azimuthal correlations and in the case of the HADES spectrometer, the parameter  $p$  is equal to  $1/6$ .

The probability to have  $n_S$  tracks in a sector is given by

$$P(n_S) = \frac{n_T!}{(n_T - n_S)!n_S!} \cdot \frac{5^{n_T - n_S}}{6^{n_T}}$$

If the minimal sector multiplicity condition of one is used, then efficiency losses result for events which have multiplicity zero in one or more of the azimuthal segments. In leading order, this probability  $W_{Loss}$  is given by the number of sectors multiplied by the probability of no tracks in a sector.

$$W_{Loss} = 6 \cdot P(n_S)|_{n_S=0} = 6 \cdot \left(\frac{5}{6}\right)^{n_T}$$

High multiplicity events are defined by efficiency losses smaller than 10%, hence  $n_T$  of these events is determined by

$$6 \cdot \left(\frac{5}{6}\right)^{n_T} \leq 0.1$$

This inequality holds for  $n_T \geq \frac{\ln 60}{\ln 60 - \ln 50}$ , i.e. for  $n_T \geq 23$ .

Taking into account the HADES solid angle of about 50%, events with maximum total multiplicity of about  $M_{Tot}^{max} \geq 50$  are defined as high multiplicity

events. Accordingly, events with  $M_{Tot}^{max} \leq 50$  are defined as medium multiplicity systems. In medium multiplicity systems, first level trigger conditions can only be applied to the total multiplicity.

Comprehensive dielectron spectroscopy of heavy-ion collisions necessitates the measurement of the dielectron signal as a function of impact parameter of the reaction. With the first level trigger approach presented here, data of central, semi-central and peripheral events can be taken by redefining the multiplicity conditions and by appropriately downscaling the resulting trigger rate. Thus, non-central events can either be downscaled and be registered simultaneously with central events or can be recorded in dedicated data taking periods. The major interest is, however, focused on central heavy-ion reactions due to the large densities reached in these collisions.

Each signal of the first level trigger has an associated deadtime due to frontend readout of detectors. This deadtime is about  $10 \mu\text{sec}$ . If the multiplicity condition is set low, then the trigger rate will be increased with a corresponding increase in probability that central events fall into the deadtime window. If, on the other hand, the multiplicity condition is set high, then central events start to get rejected due to insufficient multiplicity. For a given deadtime, there exists therefore a multiplicity condition which optimizes the number of central events which are passed onto the next trigger stage.

Due to the statistical occurrence of heavy-ion reactions, there is a finite probability that two or more events occur very close in time. Hence, TOF paddles can carry simultaneously signals of different events. The combined signals of the different events may satisfy the trigger condition whereas none of the individual events would be able to do so. This overlap probability depends strongly on the reaction rate and, thus, on beam intensity. For all of the results shown, a beam rate of  $10^8 \text{ s}^{-1}$  and a minimum bias event rate of  $10^6 \text{ s}^{-1}$  is assumed.

The performance of the first level trigger in heavy-ion collisions depends weakly on the duration of the TOF paddle signals[12,13]. If the TOF signal length is short, then the signals of the fastest particles have disappeared before the signals of the slower particles have started. The trigger system will therefore see an apparently reduced event multiplicity with increased multiplicity fluctuations. TOF signals which are long, on the other hand, result in an increased number of triggers from events overlapping in time. In this report, all the results for heavy-ion induced reactions have been derived with a TOF signal duration of 15 nsec.

## 4 First level trigger data simulation

For studying the behavior of the first level trigger, the full HADES geometry was implemented into the GEANT package[14]. A realistic field map of the toroidal magnetic field is used for tracking of the charged particles.

The collisions of the three systems studied, p+Ni, Ne+Ne and Au+Au are modeled by a transport equation of the Boltzmann-Uehling-Uhlenbeck (BUU) type. The dynamical evolution of the collisions is determined by calculating the phase space evolution for nucleons, Delta and N\* resonances. With this code, good agreement is found between data and model predictions for nucleon, pion, kaon and dilepton distributions in proton and heavy-ion induced reactions in the energy range 1-2 AGeV[15]. Since the charged particle multiplicity is mainly due to protons and pions, only these two particle species are tracked for the first level trigger simulations.

For the simulations of the first level trigger in these three systems, BUU events of different impact parameters are used. In these systems, the upper limit of the impact parameter range is defined by the geometrical cross section. In each of the three systems studied, six to eight discrete equidistant impact parameters represent the full range from zero to maximum value. Each tracked particle of an event is followed through the complete HADES geometry. A trajectory entering a TOF paddle volume defines a TOF hit. The information of this hit contains the TOF paddle number and a TOF time value. This time value represents the sum of the particles time of flight from target to the paddle hit point plus the signal propagation delay within the TOF paddle. In the left or right (LOR) timing, this signal delay is determined by the shorter of the two propagation times of the signal to either end of the paddle. In the MEAN timing, the signal propagation delay is independent of particle hit point and is equal to the propagation delay through half the length of the paddle. In the calculation of the signal propagation delay, signal time jitter or finite resolution effects are neglected. The exact TOF time value is subsequently converted into an integer format with a discretization accuracy of 10 psec and written into a CERN CWN-tupel. At this stage, each discrete impact parameter is simulated separately. Hence, separate tuple files exist for each of the discrete impact parameters simulated.

## 5 First level trigger data analysis

In the analysis of the first level trigger, a stream of events is generated by assigning a random time interval  $t_{\Delta}$  and a random impact parameter  $b$  to each event.

The time interval  $t_\Delta$  is chosen according to the probability  $p(t_\Delta) = \lambda \cdot e^{-\lambda \cdot t_\Delta}$ . This probability distribution represents the distribution of time intervals between two consecutive events, with  $\lambda$  being equal to the inverse of the average time between two consecutive events. The absolute time of an event is determined by adding  $t_\Delta$  to the absolute time of the previous event.

The impact parameter  $b$  of an event is taken from a distribution which is zero at  $b = 0$  fm and linearly increasing up to  $b = b_{max}$ . Here,  $b_{max}$  is defined by the geometrical cross section as explained above. An event is subsequently read from the tuple file with the closest nearby simulated impact parameter.

The analysis of the first level trigger loops over all TOF paddles in time steps of 1 nsec. In each loop, the sum of the TOF paddles carrying a signal at that particular moment is calculated. If the given trigger multiplicity requirement is met in a step, but not in the previous one, then a trigger transition is induced. The exact timing of the trigger transition is determined from the information of the TOF time values to within the discretization accuracy of 10 psec as described above. This trigger transition has to arrive within a trigger time window  $\Delta T_0$  as described in Section 3.1. In the prompt trigger described below, a trigger transition generates a trigger. In the delayed trigger described below, a trigger transition initiates a time window of 20 nsec during which the event has to satisfy an additional multiplicity requirement. If this additional condition is met, then a trigger is generated. Here, prompt and delayed trigger refer to the one and two step trigger approach as described in Section 8.7. Each trigger starts a deadtime window during which no other triggers are accepted.

## 6 First level trigger in p+Ni collisions

### 6.1 Minimum total multiplicity

Due to the low multiplicity of the p+Ni system, a large fraction of reactions has no tracks in one or more of the azimuthal sectors. A condition on minimal total multiplicity  $M_L \geq 2$  is therefore used in order to define the trigger. Thus, the two fastest particles of an event define the trigger.

### 6.2 Trigger timing

The dashed line in Fig. 1 shows the LOR trigger timing of p+Ni events summed over impact parameters. The time zero is the time of reaction. This timing distribution has a considerable tail at high  $\Delta T_0$  values. This tail re-

sults from events in which the second particle of the trigger condition originates from target fragmentation and is very slow. Due to these events, the signal length of the TOF paddles is taken to be 50 nsec in the p+Ni system. A TOF signal value less than 50 nsec would, in addition to the geometrical spectrometer acceptance, introduce an additional trigger efficiency factor. The systematic errors of cross section measurements are therefore minimal for a TOF signal length of 50 nsec or larger.

### 6.3 *Trigger timing of events containing dielectrons*

The width of the trigger timing shown in Fig. 1 by the dashed line results from three different sources as explained in Section 3.1. The trigger timing of dielectron events does not contain the jitter contribution due to particle velocity variations. Thus, as shown in Fig. 1 by the solid line, the trigger time jitter is reduced for dielectron events. The FWHM of this dielectron timing distribution is about 3 nsec. In Fig. 1, the events without dielectrons are downscaled with respect to the dielectron events. The relative intensity of these two classes of events is therefore arbitrary.

The timing correlation of dielectron events allows to reject trigger transitions which do not arrive within a time window  $\Delta T_0$  following the reaction. This time window  $\Delta T_0$  is defined such that about 98% of the dielectron events are contained within the window. The vertical dotted line in Fig. 1 manifests such a trigger time window. Incidentally, the boundary of this time window coincides approximately with the peak intensity of event triggers which do not contain dielectrons. Modifications of the dielectron trigger timing studied below will therefore always be compared to the timing of the peak intensity of no-pair events.

As discussed in Section 3.1, the dielectron trigger timing shown in Fig. 1 by the solid line results from trajectory length variations over the polar angle of the spectrometer and from variations in signal propagation delays in the TOF paddles. Fig. 2 displays these different trigger jitter contributions as a function of the paddle number in both the LOR and the MEAN timing approach. Low paddle numbers represent small polar angles, whereas high paddle numbers correspond to large polar angles. Shown in Fig. 2 is the TOF time information of single electrons as a function of paddle number. The diamond symbols represent the values of TOF alone, without time delays due to signal propagation in the paddles. The structure seen results from the chosen geometrical partitioning of the full polar angular range into two segments. The vertical error bars indicate the width of the TOF distribution of trajectories hitting the paddle. The data shown by the solid line represent the MEAN timing values. Here, the timing is defined by the TOF values plus the time delay introduced

by the MEAN timer. The difference between these data points and the diamond symbols is therefore proportional to the geometrical length of the TOF paddles. In these simulations, it is assumed that the MEAN timer circuit does not introduce any time jitter. The error bars of the diamond and the solid line data are therefore equal. The dashed line in Fig. 2 depicts the LOR timing. If the particle hit distribution is uniform along the length of the TOF paddles, then the LOR timing should on average contain half the propagation delay as compared to the MEAN timing. This is indeed seen in Fig. 2 where the dashed line data of the LOR timing are located about midway between the TOF only and the MEAN time data. In the LOR timing, the signal propagation delay in the TOF paddles is position dependent. This position dependency broadens the time distribution of particles hitting a paddle. The error bars of the LOR timing are therefore considerably increased with respect to the MEAN timing error bars.

The width of the trigger timing of dielectron events shown in Fig. 1 by the solid line results from folding the differential timing distribution of Fig. 2 with the polar angular distribution of the single electrons. The width of the dielectron trigger timing of Fig. 1 can be reduced by eliminating the polar angle dependence of the single electron timing shown in Fig. 2. This can be achieved by introducing an individual cable delay for each paddle. This delay ranges from zero for the largest paddle numbers to about 5 nsec for the smallest paddle numbers. We define the corrected LOR timing as the time resulting from the LOR timing corrected for the polar angle dependence by cable delays. Similarly, the corrected MEAN timing is the time from the MEAN timing corrected for the polar angle dependence by cable delays.

The upper part of Fig. 3 shows the trigger time in the corrected LOR timing approach. These data correspond to the data of Fig. 1, but with the improved trigger timing as explained above. The width of dielectron triggers is now reduced from the 3 nsec shown in Fig. 1 to about 2.5 nsec. The peak intensity of the triggers from events without dielectrons is shown by the vertical dot-dashed line. Thus, this vertical dot-dashed line represents the trigger time window  $\Delta T_0$  if no isochronous timing corrections are applied. As can be seen in this figure, the corrected LOR timing reduces the first level trigger rate due to the improved dielectron trigger time window  $\Delta T_0$ .

The lower part of Fig. 3 shows the trigger time in the corrected MEAN timing approach. The width of dielectron triggers is now reduced from the 3 nsec shown in Fig. 1 to about 0.5 nsec. As in the upper part of Fig. 3, the vertical dot-dashed and dotted lines indicate the trigger time window  $\Delta T_0$  without timing corrections and trigger time window  $\Delta T_0$  for the corrected MEAN timing, respectively. The further improved trigger time window results in a considerable rate reduction as compared to the rate resulting from the time window  $\Delta T_0$  shown in Fig. 1.

Each trigger has an associated deadtime  $T_0$  due to frontend readout of electronic channels. An event trigger occurring during the deadtime window of the previous trigger will not initiate readout and the information of the event is lost. Deadtime losses are quantified by introducing a factor  $R_{DT}$ . Thus, the first level trigger rate is given by the reaction rate multiplied by the product of trigger efficiency times  $R_{DT}$ .

As explained above, a start detector is needed for an independent measurement of the time of reaction. This independent measurement introduces an additional time jitter in the determination of the trigger timing. In the simulations presented here, the start detector time jitter has been taken into account by adding a Gaussian distributed uncertainty to the LOR and MEAN trigger timing. Table 1 lists trigger rates derived from the corrected MEAN timing for deadtimes  $T_0 = 0, 6$  and  $10 \mu\text{sec}$  and for start detector resolutions of  $\sigma_{Start} = 0.0, 0.1, 0.2$  and  $0.4 \text{ nsec}$ . Here, events with minimum total multiplicity  $M_L \geq 2$  generate a trigger. The first row shows the rates with a wide open trigger time window  $\Delta T_0 = 60 \text{ nsec}$ . As shown in Fig. 1, a condition  $\Delta T_0 = 60 \text{ nsec}$  is equivalent to no trigger window condition. The following rows display, for each value of start detector resolution, the trigger rates and  $R_{DT}$  values for trigger time windows  $\Delta T_0$  which cut the dielectron events at the 98% level (see Fig. 3). For each deadtime  $T_0$ , the rate is shown in the left column in units of  $10^5 \text{ s}^{-1}$ . The  $R_{DT}$  value is displayed in the corresponding column on the right. Without the trigger time window condition  $\Delta T_0$ , the primary rate of  $4.8 \times 10^5$  results in an  $R_{DT}$  value of 0.17 for the expected deadtime  $T_0 = 10 \mu\text{sec}$ . Here, the primary rate is defined as the rate at zero deadtime. This  $R_{DT}$  value of 0.17 indicates a first level trigger system deadtime of 83%. If the correct trigger window conditions  $\Delta T_0$  are used for the different start detector time resolutions, the primary rate of  $4.8 \times 10^5$  is reduced by a factor of about 20. For the expected values of  $T_0 = 10 \mu\text{sec}$  and  $\sigma_{Start} = 0.2 \text{ nsec}$ , for example, the  $R_{DT}$  value is equal to 0.82. Such a  $R_{DT}$  value implies a system deadtime of 18%. The system deadtime reduction from 83% to 18% represents an increase of the number of dielectron events passed to the next trigger stage by a factor of about five. Thus, the new trigger approach presented here of integrating electron identification into the first level trigger reduces the beam time requirement for the system p+Ni by a factor of about five.

## 7 First level trigger in Ne+Ne collisions

### 7.1 Trigger timing

Fig. 4 shows the timing of the trigger for Ne+Ne events of different impact parameters. Here, the trigger time is defined by the condition of minimum

total multiplicity  $M_L \geq 2$ . The time jitter contribution of the start detector is taken into account by adding a Gaussian distributed uncertainty of  $\sigma_{Start} = .2$  nsec to the trigger time. In the top part of Fig. 4, the trigger time derived from the corrected LOR timing is displayed. In the lower part, the trigger time from the corrected MEAN timing is shown. The trigger window condition  $\Delta T_0$  described in Section 3.1 is indicated in the upper and lower part by the vertical dotted lines. Such a trigger window condition  $\Delta T_0$  reduces the event rate by less than 10% in the LOR timing. In the MEAN timing, however, the event rate reduction achieved by the window condition  $\Delta T_0$  is about 40%.

### 7.2 Minimum total multiplicity

As described above, the multiplicity condition  $M_L \geq 2$  together with the trigger window condition  $\Delta T_0$  does not reduce the rate by the required factor of ten. Thus, the multiplicity condition  $M_L$  needs to be increased in order to get the necessary rate reduction. Fig. 5 shows the trigger efficiency for Ne+Ne events as a function of the total multiplicity condition  $M_L$ . Here, the trigger window condition  $\Delta T_0$  has been set wide open. The data shown in Fig. 5 represent therefore the trigger efficiency due to multiplicity selection only. Fig. 5 displays the data points for events with impact parameters of 1,2 and 3 fm, respectively. For all the impact parameters shown in Fig. 5, the efficiency exhibits a plateau of nearly 100% at low total multiplicity values but drops steeply at large values.

### 7.3 Trigger rate

Table 2 lists the trigger rates for the Ne+Ne system for deadtimes of  $T_0 = 0,6$  and  $10 \mu\text{sec}$  and for minimum total multiplicity conditions  $M_L = 2,3,4,5$  and  $6$ . As shown in Fig. 5, multiplicity conditions  $M_L > 6$  would reduce the efficiency for central events and are therefore not considered here. For each deadtime  $T_0$  in Table 2, the rate is presented on the left in units of  $10^5 \text{ s}^{-1}$  and the corresponding  $R_{DT}$  value on the right. The first two rows of Table 2 show the rates resulting from a multiplicity condition  $M_L \geq 2$ . The first row displays the rates if a wide open trigger window  $\Delta T_0$  is applied, i.e. no trigger window condition. The second row shows the rates if the correct window condition  $\Delta T_0$  is used as described in Section 3.1. The  $R_{DT}$  values of .21 and .31 indicate system deadtimes of about 80% and 70%, respectively. The following rows show the data for total multiplicity conditions  $M_L > 2$ . For these data, the event timing is determined from the two fastest particle of the event and an independent multiplicity condition  $M_L$  is required. For the expected deadtime  $T_0 = 10 \mu\text{sec}$ , for example, the multiplicity condition  $M_L \geq 6$  results in system

deadtimes of 20% and 63% with and without the trigger window condition  $\Delta T_0$ . These values represent an increase of the number of dielectron events passed to the next trigger stage by a factor of about two when applying the trigger window condition  $\Delta T_0$  derived from the corrected MEAN timing. Thus, the new trigger approach of integrating electron identification into the first level trigger reduces the beam time requirement for the system Ne+Ne by a factor of about two.

## 8 First level trigger in Au+Au collisions

Fig. 6 shows the timing of the trigger for Au+Au events of different impact parameters. Here, the trigger time is defined by the condition of minimum total multiplicity  $M_L \geq 2$ . The time jitter contribution of the start detector is taken into account by adding a Gaussian distributed uncertainty of  $\sigma_{Start} = .2$  nsec to the trigger time. The top and bottom part of Fig. 6 display the trigger time derived from the corrected LOR and MEAN timing, respectively. The trigger window condition  $\Delta T_0$  described in Section 3.1 is indicated in the upper and lower part by the vertical dotted lines. Due to abundantly produced pions, such a trigger window condition  $\Delta T_0$  has very little effect in the high multiplicity system Au+Au. In this system, a first level trigger has to be based on multiplicity selection only.

### 8.1 Sector multiplicity condition

In the high multiplicity system Au+Au, a multiplicity condition in each azimuthal sector will tag central events. Fig. 7 shows the tagging efficiency for this system as a function of the imposed sector multiplicity condition  $M_S$ . This condition implies that the charged particle multiplicity is greater or equal to  $M_S$  in each of the six azimuthal sectors. Shown are the data points for events with impact parameters of 1,3 and 5 fm, respectively. For all the impact parameters shown in Fig. 7, the efficiency exhibits a plateau of nearly 100% at low sector multiplicity values but drops steeply at large multiplicity values. The optimal choice for the sector multiplicity condition is a value as large as possible but still within the plateau of the impact parameter  $b = 1$  fm. Hence, the sector multiplicity condition is set to  $M_S \geq 8$  for the calculations shown below.

## 8.2 Trigger timing

Events satisfying the sector multiplicity condition  $M_S$  generate a trigger transition. The delay of this signal relative to the time of reaction and the signal jitter are of interest. Fig. 8 shows the corrected MEAN time of the trigger transition for events with different impact parameters. Here, the two fastest particle in each azimuthal sector define the sector timing. The trigger time is then defined by the one of the six sector timings which arrives last. Central events are represented by the solid line. The FWHM of their time distribution amounts to about 1 nsec. The FWHM value for events with impact parameters of 3 and 5 fm are about 1.2 and 1.5 nsec, respectively. Semi-central events meet the condition  $M_L \geq 2$  for the sector timing only with the help of slower moving particles. Hence, for increasing impact parameters, a shift of the centroid to larger time values as well as a broadening of the distribution is seen. The time zero in Fig. 8 is the time of reaction.

## 8.3 Total multiplicity

The sector multiplicity requirement defines a condition on minimum particle multiplicity in each of the six azimuthal sectors. A condition on minimum total multiplicity might further reduce non-central events while at the same time accepting all central events. At the moment of the trigger transition, the total multiplicity for central events is still building up, whereas it is almost exhausted for non-central events. Fig. 9 displays the maximum total multiplicity reached during a time window of 20 nsec following the trigger transition. Central and non-central events which satisfy the sector multiplicity condition  $M_S \geq 8$  behave quite differently in Fig. 9. A condition on minimum total multiplicity will therefore further reduce non-central events.

## 8.4 Timing total multiplicity

Fig. 10 shows the time at which the maximum event multiplicity is reached for events with impact parameters  $b=1,3$  and 5 fm. Here, the time zero is the time of the trigger transition defined by the sector multiplicity condition  $M_S$ . For central events, the maximum total multiplicity develops between 5 and 15 nsec following the trigger transition. Non-central events with impact parameters  $b=5$  fm develop their maximum total multiplicity during a time span of about 10 nsec following the trigger transition. Hence a time window of 15-20 nsec duration following the trigger transition seems adequate to test for the maximum total event multiplicity.

### 8.5 Trigger efficiency

Each trigger transition followed by a total multiplicity larger than a required minimum value  $M_T$  generates a trigger. Each trigger has an associated deadtime due to frontend readout of electronic channels. An event trigger occurring during the deadtime window of the previous trigger will not initiate readout and the information of the event is lost. Fig. 11 shows the values of  $\text{Eff}_{LV1} \times R_{DT}$  for central events for  $M_S \geq 8$  as a function of the required total multiplicity  $M_T$ . Here,  $\text{Eff}_{LV1}$  denotes the first level trigger efficiency, i.e., the efficiency for zero deadtime.  $R_{DT}$  is a reduction factor which contains the effects of the trigger deadtime. For the deadtime of  $T_0 = 10 \mu\text{sec}$ , the  $\text{Eff}_{LV1} \times R_{DT}$  value has a maximum at an  $M_T$  value of about 110. At lower  $M_T$  values, semi-central events do not get suppressed efficiently. Thus, the increased rate of semi-central events leads to a decrease of the  $\text{Eff}_{LV1} \times R_{DT}$  values of central events. For high  $M_T$  values,  $\text{Eff}_{LV1} \times R_{DT}$  decreases since central events start to get rejected due to insufficient multiplicity. The data for the deadtime of  $T_0 = 6 \mu\text{sec}$  are shown for comparison.

### 8.6 Trigger rate

Table 3 lists the trigger rates in units of  $10^5 \text{ s}^{-1}$  for the different total multiplicity thresholds  $M_T$  and for deadtimes of  $T_0 = 0,6$  and  $10 \mu\text{sec}$ , respectively. A first level trigger rate of  $1. \times 10^5 \text{ s}^{-1}$  is the input design value for the next trigger stage. Each value of  $T_0$  in Table 3 corresponds to two columns. The left column shows the rate of trigger transitions resulting from the sector multiplicity condition  $M_S \geq 8$ . The right column displays the rate if additionally the total multiplicity condition  $M_T$  is required.

Table 4 lists the partial trigger rates from events of different impact parameters. For the chosen multiplicity requirements, triggers from events with impact parameters  $b \geq 5 \text{ fm}$  are negligible and therefore not listed in Table 4. Both impact parameters  $b = 1$  and  $3 \text{ fm}$  correspond to two columns. On the left, the partial trigger rate is shown in units of  $10^5 \text{ s}^{-1}$ . On the right, the partial rates are normalized to the total trigger rate and shown in units of percent.

### 8.7 First level trigger based on $M_T$

The trigger scheme studied so far for the system Au+Au divides the first level trigger into two consecutive steps: In a first step, a condition  $M_S$  on minimum number of particles in each sector establishes a trigger transition. In a second step, the trigger transition is asserted or rejected within a subsequent

time window depending on whether the total multiplicity condition  $M_T$  is satisfied. However, a one step trigger scheme, based exclusively on the total multiplicity  $M_T$ , seems also feasible since the total multiplicity condition  $M_T$  is more restrictive than the sector multiplicity condition  $M_S$ . Fig. 12 displays the trigger time achieved by the one and two step trigger. The data shown in Fig. 12 represent the timing of all events which generate a trigger, irrespective of impact parameter. This trigger time is shown for the LOR and corrected MEAN timing in the upper and lower part, respectively. The solid line shows the timing in the two step scheme with conditions  $M_S \geq 8$  and  $M_T \geq 110$  as explained above. These solid line data points correspond to Fig. 8 with the additional condition of total multiplicity  $M_T$ . The FWHM of this distribution is about 1 nsec. The dashed line in the lower part of Fig. 12 represents the corrected MEAN timing in the one step trigger. Here, the trigger time is defined by the timing of the particle for which the total multiplicity condition  $M_T \geq 110$  becomes true. As expected, the timing is delayed compared to the two step trigger and considerably broadened. The FWHM of this distribution is about 6 nsec. The upper part of Fig. 12 displays the corresponding data in the LOR timing. Similarly as in the corrected MEAN time, the trigger time in the one step trigger approach is delayed and broadened.

## 9 Conclusions

A novel approach for a dielectron trigger improves the first level trigger performance considerably. This new approach achieves electron identification by using isochronous TOF information. The proposed first level trigger architecture combines TOF conditions for the two fastest particles of the event with multiplicity requirements. The chosen TOF conditions result in a single electron efficiency of 99%. Simulations which take the HADES spectrometer as an example show that this new approach reduces the beam time requirement by a factor of five in the low multiplicity system p+Ni and by a factor of two in the medium multiplicity system Ne+Ne. In the high multiplicity system Au+Au, a first level trigger based exclusively on multiplicity can be implemented in both a one or two step trigger architecture. By judicious choice of multiplicity conditions, the number of central collisions passed onto the next trigger stage can be maximized.

## Acknowledgements

The support of the electron group at GSI and, in particular, fruitful discussions with W.Koenig are gratefully acknowledged. The authors thank Gy. Wolf for

providing the BUU data files used in the simulations.

## References

- [1] Workshop on Dilepton Production in Relativistic Heavy-Ion Collisions, GSI 1994, ed. H. Bokemeyer.
- [2] International Workshop on Soft Dilepton Production, LBNL 1997, org. J. Carroll, V. Koch, H. Matis.
- [3] A. Yegneswaran et al., Nucl. Instr. and Meth. A 290 (1990) 61.
- [4] T.F. Günzel et al., Nucl. Instr. and Meth. A 316 (1992) 259.
- [5] S. Beedoe et al., Phys. Rev. C 47 (1993) 2840.
- [6] R. Baur et al., Nucl. Instr. and Meth. A 343 (1994) 87.
- [7] R. Gernhäuser et al., Nucl. Instr. and Meth. A 371 (1996) 300.
- [8] The HADES collaboration, Proposal for a High Acceptance Dielectron Spectrometer, GSI 1994.
- [9] A.R. Gabler et al., Nucl. Instr. and Meth. A 346 (1994) 168.
- [10] R. Schicker et al., Nucl. Instr. and Meth. A 380 (1996) 586.
- [11] M. Axiotis, diploma thesis, University of Cyprus, 1997.
- [12] R. Schicker and H. Tsertos, University of Cyprus preprint UCY-96/04.
- [13] R. Schicker and H. Tsertos, University of Cyprus preprint UCY-96/08.
- [14] H. Schön, PhD thesis, University of Frankfurt, 1996.
- [15] G. Wolf, W. Cassing and U. Mosel, Nucl.Phys. A552 (1993) 549.

## Tables

$\sigma_{Start}$ [nsec]	Window $\Delta T_0$ [nsec]	$T_0 = 0 \mu\text{sec}$		$T_0 = 6 \mu\text{sec}$		$T_0 = 10 \mu\text{sec}$	
		rate[ $10^5$ ]	$R_{DT}$	rate[ $10^5$ ]	$R_{DT}$	rate[ $10^5$ ]	$R_{DT}$
	60.0	4.78	1.0	1.25	0.26	0.83	0.17
0.0	14.1	0.19	1.0	0.17	0.90	0.16	0.84
0.1	14.1	0.19	1.0	0.17	0.92	0.16	0.83
0.2	14.2	0.22	1.0	0.20	0.90	0.18	0.82
0.4	14.4	0.28	1.0	0.24	0.85	0.22	0.78

Table 1

Trigger rates from corrected MEAN timing in the system p+Ni for deadtimes  $T_0 = 0, 6$  and  $10 \mu\text{sec}$ . In the left column, the rates are shown in units of  $10^5 \text{ s}^{-1}$ . In the right column, the deadtime reduction factor  $R_{DT}$  is shown. The first row shows the rate without trigger time window condition. Subsequent rows show the rates if the correct window condition  $\Delta T_0$  is applied.

$M_L$	Window $\Delta T_0$ [nsec]	$T_0 = 0 \mu\text{sec}$		$T_0 = 6 \mu\text{sec}$		$T_0 = 10 \mu\text{sec}$	
		rate[ $10^5$ ]	$R_{DT}$	rate[ $10^5$ ]	$R_{DT}$	rate[ $10^5$ ]	$R_{DT}$
2	60.0	3.81	1.0	1.71	0.31	0.80	0.21
	14.2	2.23	1.0	0.95	0.43	0.69	0.31
3	60.0	3.03	1.0	1.09	0.36	0.76	0.25
	14.2	1.36	1.0	0.75	0.55	0.58	0.43
4	60.0	2.50	1.0	1.01	0.40	0.72	0.29
	14.2	0.81	1.0	0.55	0.68	0.45	0.56
5	60.0	2.09	1.0	0.94	0.45	0.68	0.33
	14.2	0.48	1.0	0.37	0.78	0.32	0.67
6	60.0	1.75	1.0	0.86	0.49	0.64	0.37
	14.2	0.26	1.0	0.23	0.86	0.21	0.80

Table 2

Trigger rates from corrected MEAN timing in the system Ne+Ne for deadtimes  $T_0 = 0, 6$  and  $10 \mu\text{sec}$  and for total multiplicity conditions  $M_L = 2, 3, 4, 5$  and  $6$ . In the left column, the rates are shown in units of  $10^5 \text{ s}^{-1}$ . In the right column, the deadtime reduction factor  $R_{DT}$  is shown. For each multiplicity  $M_L$ , the first and second row show the rates without and with trigger time window condition.

Au + Au	$T_0 = 0 \mu\text{sec}$		$T_0 = 6 \mu\text{sec}$		$T_0 = 10 \mu\text{sec}$	
	rate [ $10^5$ ]		rate [ $10^5$ ]		rate [ $10^5$ ]	
$M_T \geq 100$	1.08	0.37	0.90	0.31	0.80	0.28
$M_T \geq 105$	1.08	0.28	0.94	0.24	0.85	0.22
$M_T \geq 110$	1.08	0.19	0.98	0.17	0.91	0.16
$M_T \geq 115$	1.08	0.13	1.01	0.12	0.97	0.12
$M_T \geq 120$	1.09	0.08	1.04	0.08	1.01	0.07

Table 3

Rates of first level trigger transitions (left column) and of triggers (right column) in the system Au+Au (see text). The rates are shown in units of  $10^5 \text{ s}^{-1}$  for deadtimes  $T_0 = 0, 6$  and  $10 \mu\text{sec}$  and for different total multiplicity conditions  $M_T$ .

Au + Au	rate b=1fm		rate b=3 fm	
	[ $10^5$ ]	[%]	[ $10^5$ ]	[%]
$M_T \geq 100$	0.11	39.7	0.17	59.8
$M_T \geq 105$	0.11	51.0	0.11	48.6
$M_T \geq 110$	0.11	69.5	0.05	29.9
$M_T \geq 115$	0.09	80.3	0.02	19.0
$M_T \geq 120$	0.07	90.3	0.01	8.7

Table 4

First level partial trigger rates of events with impact parameters  $b = 1$  and  $3 \text{ fm}$  in the system Au+Au for different total multiplicity conditions  $M_T$ . The left column displays the partial rate in units of  $10^5 \text{ s}^{-1}$ . In the right column, the partial rates are normalized to the total trigger rate and shown in units of percent.

## Figure Captions

Fig. 1. LOR trigger time from the two fastest particle of the event. The solid line shows the data of dielectron events. The dashed line displays the data for p+Ni events which do not contain dielectrons. The vertical dotted line represents the dielectron TOF condition.

Fig. 2. TOF data for single electron trajectories as a function of paddle number. The diamond symbols represent the TOF values alone. The solid and dashed line data represent the time in the LOR and MEAN timing approach, respectively.

Fig. 3. Corrected LOR and MEAN trigger time from the two fastest particle of the event are shown in the upper and lower part, respectively. The solid and dashed line data represent dielectron events and no-pair p+Ni events, respectively. The vertical lines indicate the dielectron TOF conditions (see text).

Fig. 4. The trigger time from the two fastest particle of Ne+Ne events for impact parameters  $b=1,3$  and  $5$  fm. The corrected LOR and MEAN timing are shown in the upper and lower part, respectively. The vertical dotted lines indicate the trigger window condition  $\Delta T_0$ .

Fig. 5. Trigger efficiency for the system Ne+Ne at 2 AGeV as a function of the minimum total multiplicity  $M_L$ . Shown are data points for events with impact parameters of  $b=1,2$  and  $3$  fm.

Fig. 6. The trigger timing from the two fastest particle of Au+Au events for impact parameters  $b=1,3$  and  $5$  fm. The corrected LOR and MEAN timing are shown in the upper and lower part, respectively. The vertical dotted lines indicate the trigger window condition  $\Delta T_0$ .

Fig. 7. First level trigger efficiency for the system Au+Au at  $1$  AGeV as a function of the minimum sector multiplicity  $M_S$ . Shown are data points for events with impact parameters of  $b=1,3$  and  $5$  fm.

Fig. 8. Corrected MEAN trigger time in the Au+Au system derived from sector timings of the two fastest particles in each sector(see text). Shown are the data for impact parameters  $b=1,3$  and  $5$  fm. The time zero is the time of reaction.

Fig. 9. The maximum total Au+Au event multiplicity for impact parameters  $b=1,3$  and  $5$  fm reached during a time window of  $20$  nsec following the trigger transition.

Fig. 10. Time at which maximum total event multiplicity is reached for impact parameters  $b=1,3$  and  $5$  fm. The time zero is the time of trigger transition.

Fig. 11. Efficiency of first level trigger (deadtime losses included) for central events. Shown are the data points as a function of the total multiplicity condition  $M_T$  for deadtimes of  $0,6$  and  $10$   $\mu$ sec.

Fig. 12. Trigger timing in the one (dashed line) and two step (solid line) trigger scheme (see text). The data in the LOR and corrected MEAN timing are shown in the upper and lower part, respectively. The time zero is the time of reaction.

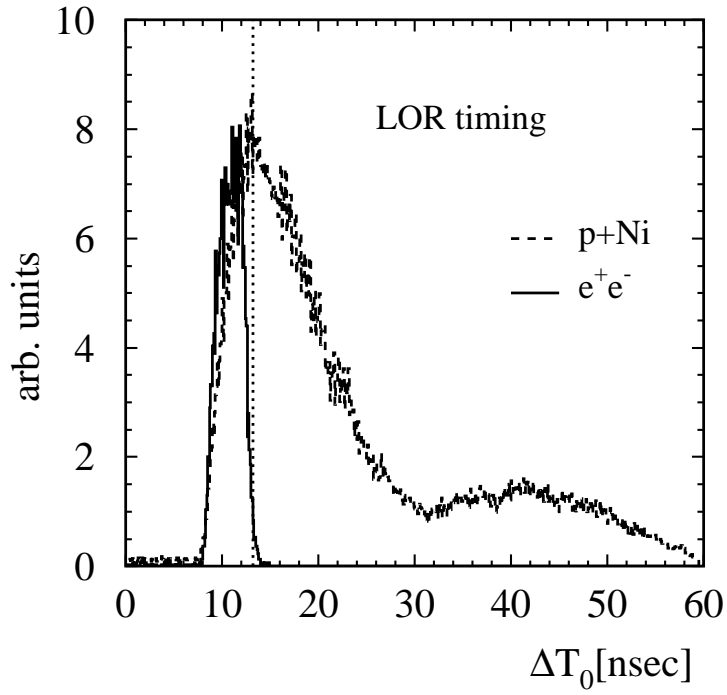


FIG.1

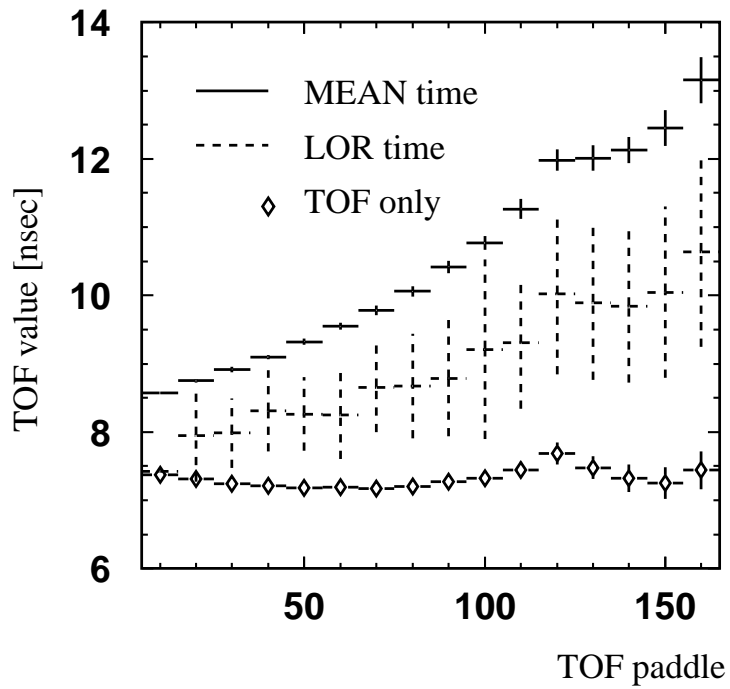


FIG.2

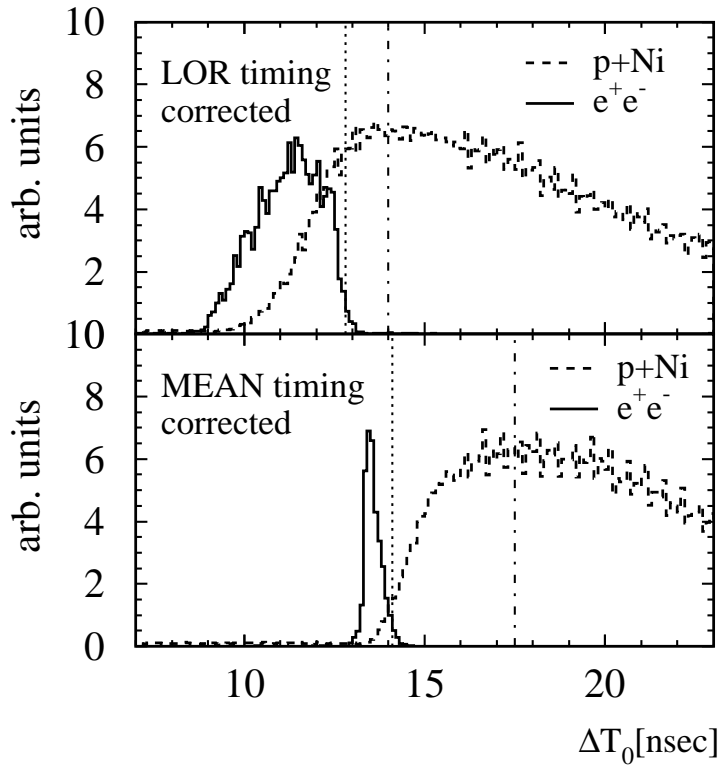


FIG.3

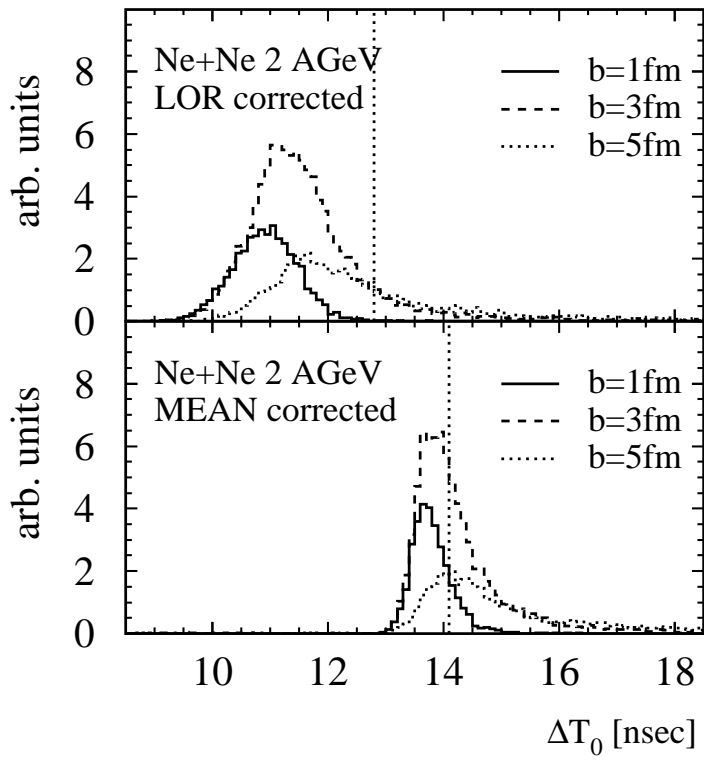


FIG.4

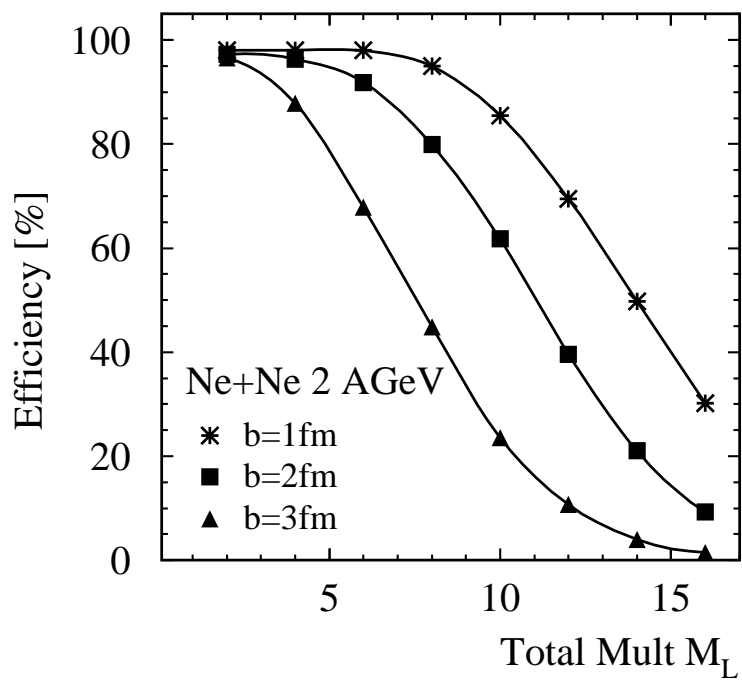


FIG.5

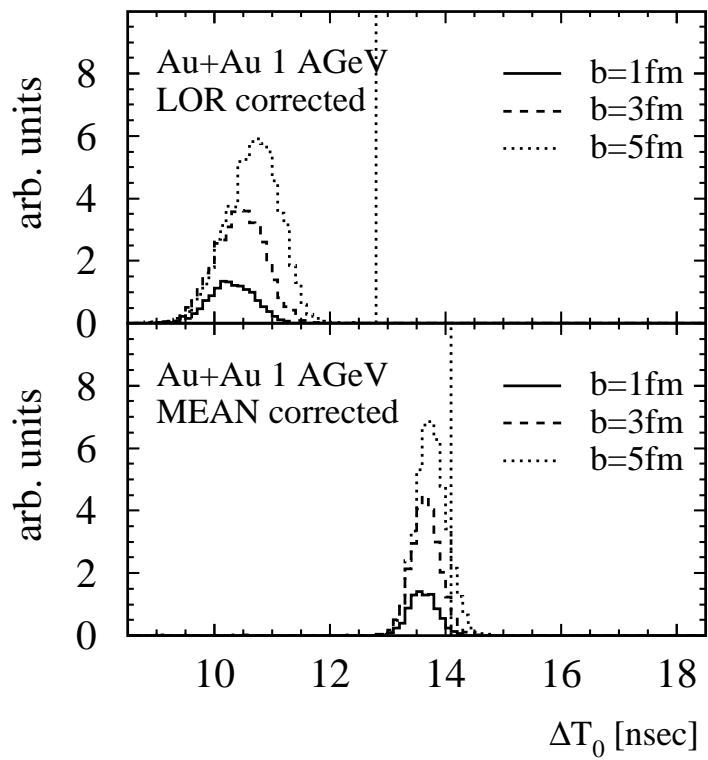


FIG.6

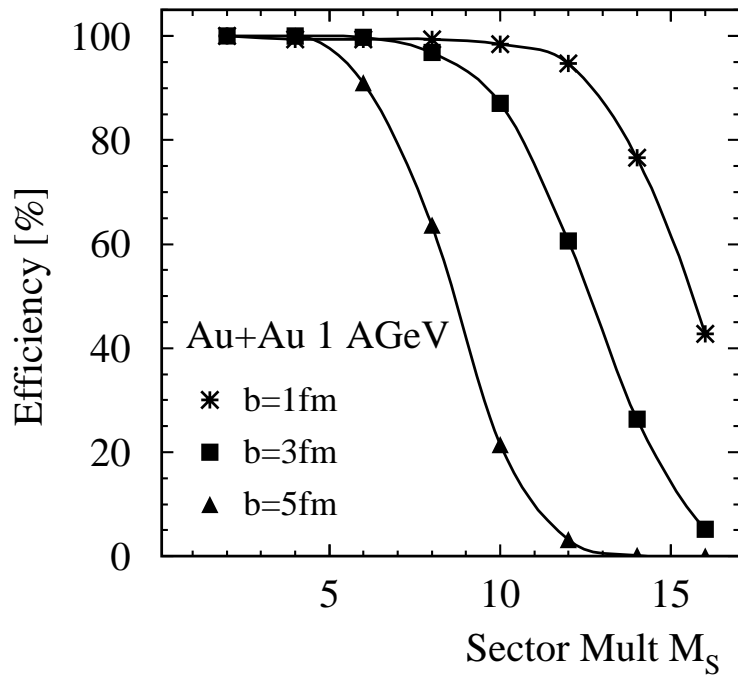


FIG.7

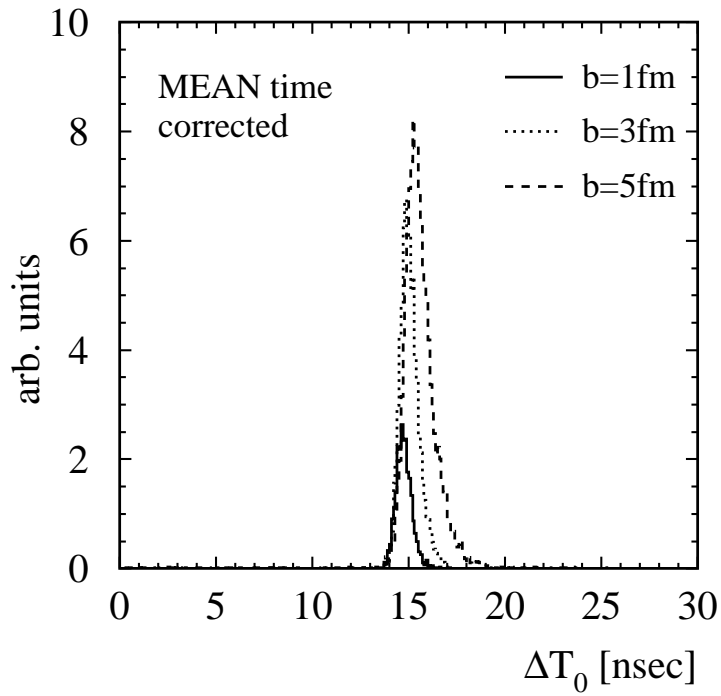


FIG.8

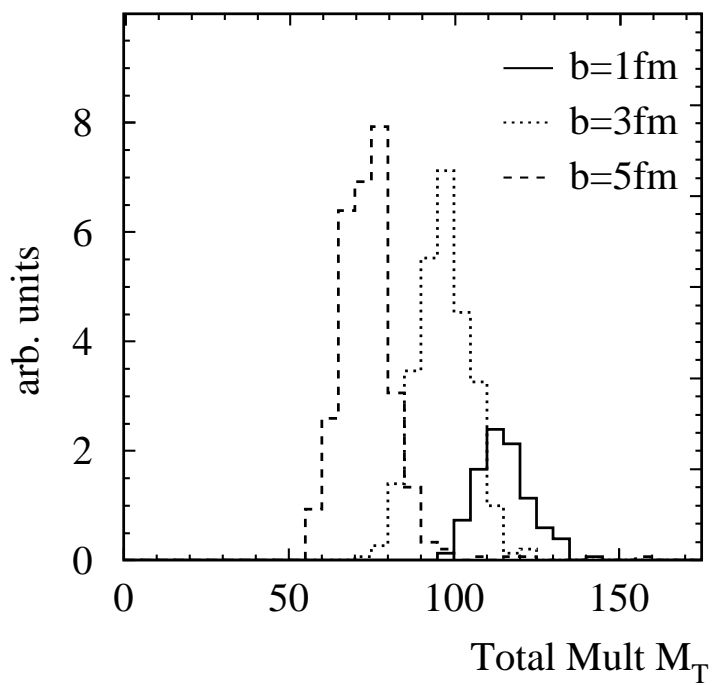


FIG.9

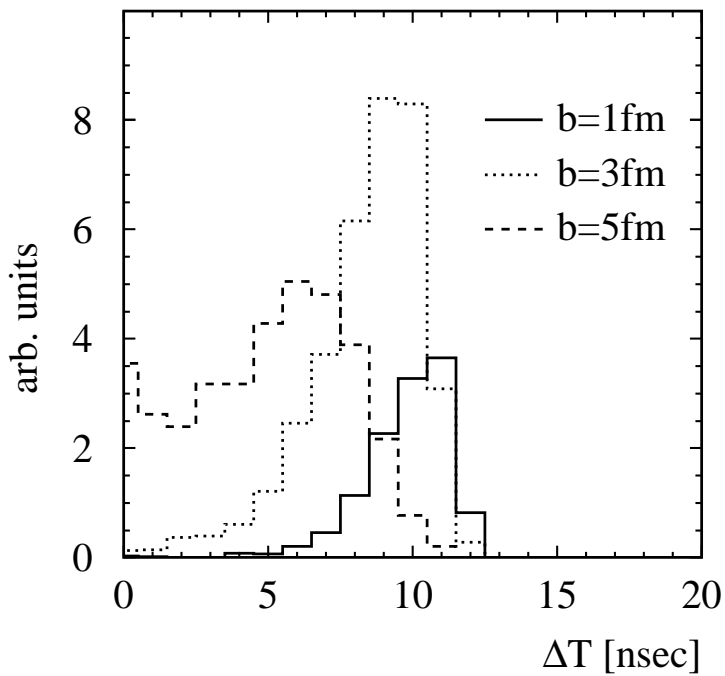


FIG.10

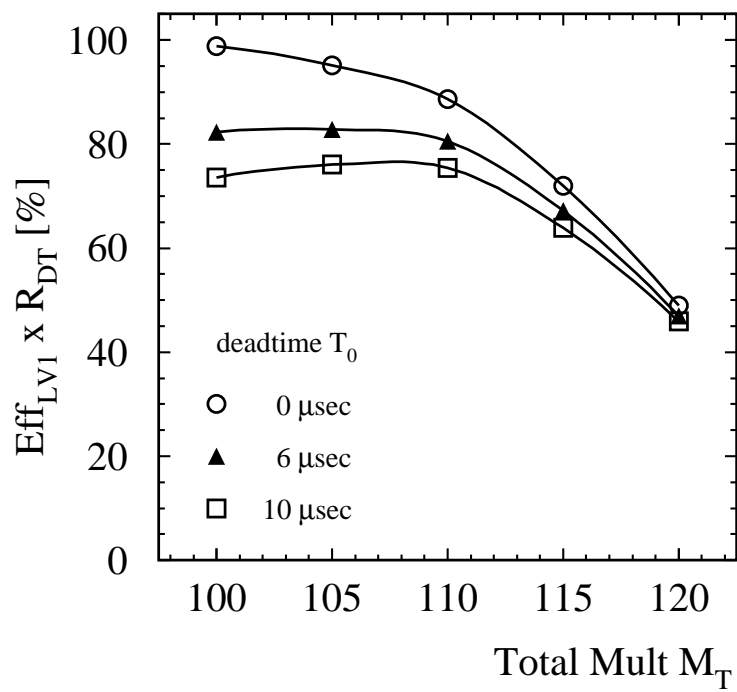


FIG.11

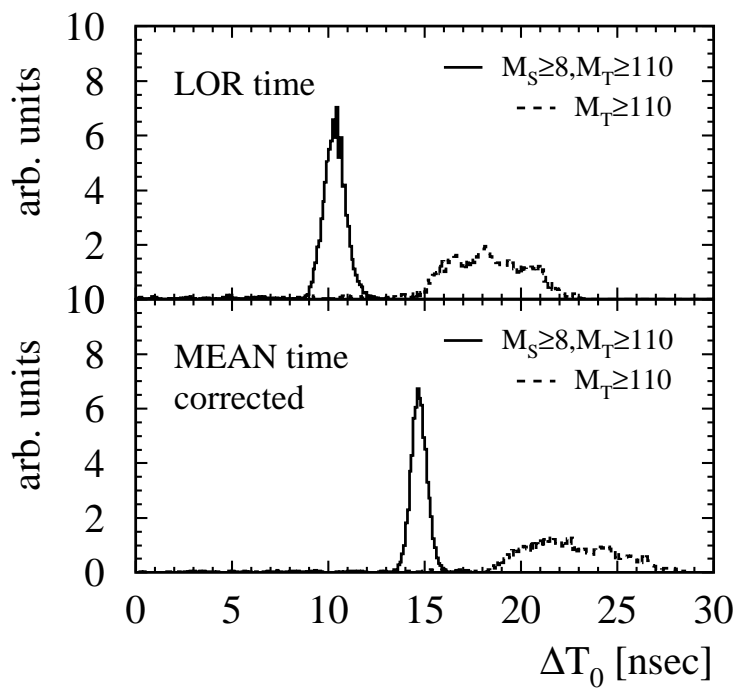


FIG.12